

Article

The Effect of Organic Spacer Cations with Different Chain Lengths on Quasi-Two-Dimensional Perovskite Properties

Lei Zhang ¹, Mingze Xia ², Yuan Zhang ¹, Li Song ³, Xiwei Guo ³, Yong Zhang ¹, Yulei Wang ¹ and Yuanqin Xia ^{1,*}

¹ Hebei Key Laboratory of Advanced Laser Technology and Equipment, School of Electronics and Information Engineering, Hebei University of Technology, 5340 Xiping Road, Tianjin 300401, China; zl98nian@163.com (L.Z.); zhangyuan956912516@163.com (Y.Z.); zhangyong@hebut.edu.cn (Y.Z.); wyl@hebut.edu.cn (Y.W.)

² Cnooc Energy Technology and Services, Tianjin 300450, China; xiamz2023@163.com

³ Tianjin Key Laboratory of Electronic Materials and Devices, School of Electronics and Information Engineering, Hebei University of Technology, 5340 Xiping Road, Tianjin 300401, China; songli@hebut.edu.cn (L.S.); g17634324378@163.com (X.G.)

* Correspondence: xia yq@hebut.edu.cn

Abstract: In the past 20 years, perovskite-related research has attracted wide attention. The related research into two-dimensional/quasi-two-dimensional perovskite has propelled the research of perovskite materials to a new height. To improve the properties of quasi-2D perovskite, improve the stability of materials, and achieve specific functions, using different types, volumes, and lengths of organic spacers is an essential method. In this paper, quasi-2D perovskites with EDA (ethylene diammonium), PDA (1,3-propanediammonium), and BDA (1,4-butanediammonium) ($m = 2-4$) as organic spacers were prepared, and the effects of different organic spacers on the 2D perovskite were investigated. The results show that the length of the organic spacer significantly impacts the perovskite's properties. A shorter organic spacer can effectively reduce the quantum confinement and dielectric confinement in perovskite. It should be noted that if the organic spacer is too short, the stability of the quasi-2D perovskite will be greatly reduced.

Keywords: quasi-2D perovskite; transient absorption spectra; carrier dynamics



Citation: Zhang, L.; Xia, M.; Zhang, Y.; Song, L.; Guo, X.; Zhang, Y.; Wang, Y.; Xia, Y. The Effect of Organic Spacer Cations with Different Chain Lengths on Quasi-Two-Dimensional Perovskite Properties. *Inorganics* **2024**, *12*, 12. <https://doi.org/10.3390/inorganics12010012>

Academic Editor: Chiara Dionigi

Received: 24 October 2023

Revised: 17 December 2023

Accepted: 18 December 2023

Published: 27 December 2023



Copyright: © 2023 by the authors. Licensee MDPI, Basel, Switzerland. This article is an open access article distributed under the terms and conditions of the Creative Commons Attribution (CC BY) license (<https://creativecommons.org/licenses/by/4.0/>).

1. Introduction

With the development of human society, the living standard of human beings is constantly improving, accompanied by the rapid consumption of energy. The utilization of renewable energy has become an important way to solve this problem. Perovskite is starting to attract attention in this context. Because of its excellent performance and low cost, it has become the research hotspot of many scholars. It has shown a broad application prospect in many fields, such as solar cells [1–10], LEDs [11–21], and so on. In order to make perovskite materials achieve specific functions and improve their efficiency, it is very important to understand the carrier dynamics of perovskite materials, which have an important guiding role.

In order to obtain high-stability and high-efficiency perovskite materials, research on 2D/quasi-2D perovskite has been an important direction. The basic properties of Dion–Jacobson (DJ) perovskite are usually determined by organic spacer cations [22–24]. Among these organic spacer cations, diammonium is the most widely studied, including linear cations [25,26] and ring cations [27–29]. The ammonium cation of an organic spacer cation can form hydrogen bonds with multiple ends of the inorganic octahedral structure, so factors such as the spatial configuration and length of the organic spacer cation are crucial to the structure and size of perovskite [30–32]. It also directly affects the distortion of the inorganic layer connected by the organic spacer [33,34]. In contrast to three-dimensional perovskite, quasi-2D perovskite has quantum confinement and dielectric

confinement [35–37]. The quantum confinement and dielectric confinement lead to a degradation of the properties of quasi-2D perovskite. There are two ways to solve this problem: using a shorter and higher-dielectric-constant organic isolation layer [38] or improving the cross-layer charge transfer [39]. It has been found that large organic alkyl ammonium cations can achieve a uniform distribution of quantum wells (QWs) in perovskite and create a flat energy landscape [40]. Kanatzidis studied DJ-type perovskites with organic spacers of different chain lengths ($m = 4-9$) and proved that the carbon chain length of alkyl diammonium cations can affect the optical properties of perovskite materials by adjusting the spacing between inorganic layers [41]. Using smaller organic spacer cations instead of larger organic spacer cations in order to shorten the distance between inorganic layers can effectively weaken the quantum confinement effect in perovskite [42]. In other aspects, Ahmacl et al. [43] and Zheng et al. [44] used organic isolation layers to adjust and control the crystallinity, charge mobility, QW width, and distribution of aligned 2D perovskites. However, researchers still lack understanding regarding the effect of organic spacers of different lengths on quasi-2D perovskites. The internal mechanisms of quasi-2D perovskite properties (such as the energy-transfer processes) induced by different organic spacers still need to be further explored.

In order to further explore the effects of different organic spacer cations on the carrier dynamics of quasi-2D perovskite, we prepared quasi-2D perovskite thin films with CsPbBr_3 as a matrix and EDA^{2+} (ethylene diammonium), PDA^{2+} (1,3-propanediammonium), and BDA^{2+} (1,4-butanediammonium) as organic spacer cations. As shown in Figure 1, perovskites with different n values also have some differences in structure. The quasi-2D perovskite film used in this paper is made using the spin-coating method, and the n value is four.

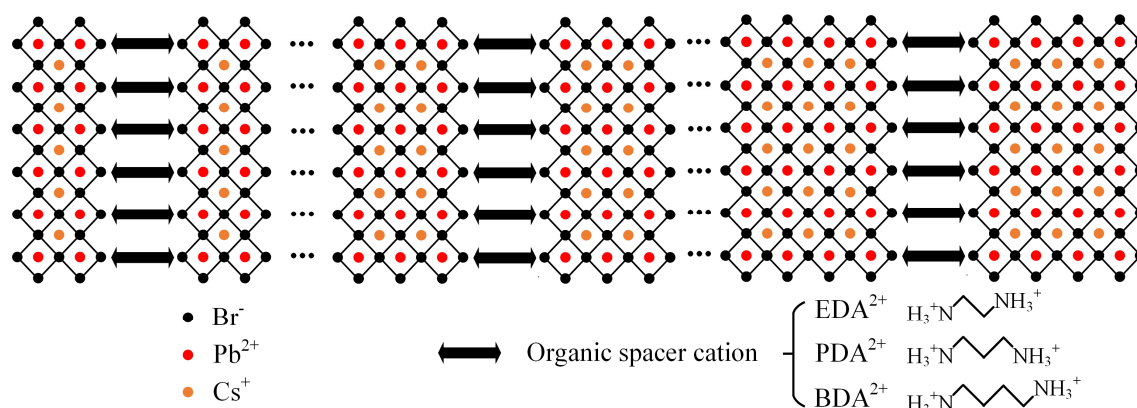


Figure 1. $\text{EDACs}_3\text{Pb}_4\text{Br}_{13}$, $\text{PDACs}_3\text{Pb}_4\text{Br}_{13}$, and $\text{BDACs}_3\text{Pb}_4\text{Br}_{13}$ diagram of multi-n phase structure.

2. Results

In this study, the films of $\text{EDACs}_3\text{Pb}_4\text{Br}_{13}$, $\text{PDACs}_3\text{Pb}_4\text{Br}_{13}$, and $\text{BDACs}_3\text{Pb}_4\text{Br}_{13}$ are denoted as EDA, PDA, and BDA, respectively. The composition and content of quasi-2D perovskite were examined using ultraviolet–visible spectroscopy (UV–Vis absorption spectrum).

Figure 2a illustrates the exciton absorption signals of EDA, PDA, and BDA. Notably, a prominent exciton absorption peak is observed near 480 nm in all three samples. This specific exciton absorption peak signal aligns with the absorption characteristics of the four-dimensional phase ($n = 4$) [40].

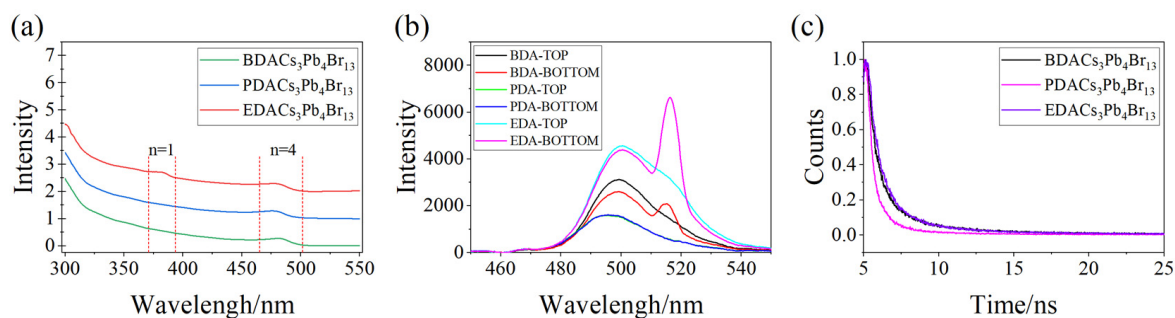


Figure 2. EDACs₃Pb₄Br₁₃, PDACs₃Pb₄Br₁₃, and BDACs₃Pb₄Br₁₃ (a) UV–Vis absorption spectra. (b) PL spectra. (c) TRPL spectra.

In perovskite materials, the notation $n = 4$ signifies the presence of the $n = 4$ phase within the perovskite film, indicating that the film consists of four inorganic layers. This designation holds for any other value of n as well. Notably, the exciton absorption peaks at 480 nm for the $n = 4$ phase in different organic spacers are nearly identical, suggesting their four-dimensional phase band gaps are closely aligned. Moreover, the EDA film sample exhibits a notable exciton absorption peak at 381 nm, corresponding to the one-dimensional phase absorption of the EDA film. In forming a DJ-type perovskite, the precursor solution is tailored according to the specific n value desired for the perovskite. It is worth noting that other dimensional phase components may also emerge in the final production of perovskite. While the UV–Vis spectra do not show exciton absorption signals of other dimensional phases, this does not imply the absence of low-dimensional phase components in quasi-2D perovskite films. These findings suggest that the enhanced interlayer interaction in EDA, PDA, and BDA films mitigates the quantum confinement effect in the quasi-2D phase. Furthermore, short-chain organic spacers in EDA effectively reduce the distortion of DJ-type perovskite [45–47]. The quantum confinement effect (QCE) is a phenomenon in which the quantization of energy in microscopic particles becomes more pronounced as the spatial confinement of their motion decreases. In the context of electrons in a solid, when at least one dimension in the three-dimensional scale reaches the nanometer scale, the movement of electrons in that dimension becomes restricted, leading to the manifestation of quantum effects. This confinement results in an increase in the energy-level band gap. In the case of perovskite films, this effect leads to a uniform distribution of QWs. Comparing RP perovskite with DJ perovskite, it is noted that DJ perovskite has fewer organic spacers. This reduction in organic spacers is suggested as one of the reasons why the exciton absorption peak of DJ perovskite is not as prominent.

Additionally, subtle differences exist despite the close proximity of the $n = 4$ exciton absorption peaks in quasi-2D organic spacer cations of perovskite films. Specifically, the $n = 4$ phase exciton absorption peak of PDA exhibits a 4 nm blue shift compared to the other two samples. Examining the exciton absorption of EDA at 380 nm in UV–Vis spectra, it is observed that EDA demonstrates higher exciton absorption at 380 nm. This suggests that EDA²⁺, compared to PDA²⁺ and BDA²⁺, can promote the formation of a low-dimensional phase with small n values.

The exciton absorption peaks of perovskite films are initially observable through UV–Vis spectroscopy, providing valuable information on the absorption characteristics of the sample. In Figure 2b, the photoluminescence (PL) spectra of quasi-2D perovskite films with different organic spacer cations are presented. The three samples are excited from the top, and the PL spectra collected from the bottom of the perovskite film are analyzed. The PL spectrum signal exhibits two main parts. First, there is a broad peak near 500 nm in the left part of the spectrum. Combined with UV–Vis spectra, it can be deduced that this broad peak corresponds to the fluorescence signal of the $n = 4$ phase. The second part is a narrow peak near 525 nm in the right part of the spectrum. This peak is attributed to the amplified spontaneous emission (ASE) signal of the quasi-2D perovskite samples. The ASE signal in the PL spectrum is produced by the bulk phase

formed in quasi-2D perovskite. In the excited state, carriers spontaneously radiate to the ground state, releasing photons. The energy of these photons corresponds to the energy difference between the excited-state carrier and the ground-state carrier. The photons produced by spontaneous emission can induce stimulated emission of carriers in the bulk phase, and the effect is that the spontaneous emission signal is amplified, and, thus, the ASE signal is produced. Although the ASE signal contains stimulated radiation, it is still spontaneous radiation in nature. The amplification of spontaneous emission is directly related to the number of particles in the upper energy level. From the PL spectra, EDA perovskite film samples are more likely to produce an ASE signal than BDA and PDA samples. This is because the energy transfer in EDA film samples is more intense and smoother. The carrier in the $n = 4$ phase can transfer into the bulk phase rapidly and effectively. The carrier number can be rapidly accumulated in the bulk phase. Compared to the PL spectrum without an ASE signal, the decrease in the fluorescence signal of the $n = 4$ phase when the ASE signal is generated also proves this point. From the PL spectra, it can be seen that the ASE signal is more easily generated by the excitation of the quasi-2D perovskite samples from the bottom. The energy-transfer process from the low-dimensional phase to the bulk phase at the bottom of perovskite films is better than that at the top of the perovskite film. We attribute this phenomenon to the higher density of states at the bottom of perovskite films. This is due to the deposition of partial phases on the bottom of the films under gravity during spin coating. The next experiments will also prove it.

In Figure 2b, the PL spectra of the perovskite films reveal a notable blue shift of 4 nm in the PL emission peak of PDA perovskite films compared to BDA and EDA. This shift aligns with the findings from the UV–Vis spectra. The origin of this phenomenon is the distortion of the perovskite lattice induced by PDA^{2+} organic spacer cations. The distortion alters the Pb–Br bond length in quasi-2D perovskite, resulting in a modification of the perovskite's band gap to some extent. Referencing the literature [48], when the organic spacer cations are PDA^{2+} , the distortion in the perovskite is more pronounced compared to with BDA^{2+} and EDA^{2+} organic spacer cations. For PDA, this substantial lattice distortion is responsible for the observed blue shift in the PL spectral emission peak. Furthermore, this lattice distortion is also responsible for the weak $n = 4$ phase fluorescence signal of PDA. When the organic spacer cations are BDA^{2+} and EDA^{2+} , the perovskite lattice also undergoes distortion, albeit less severely than with PDA^{2+} . Consequently, the band gap of the $n = 4$ phase experiences minimal change. Notably, EDA^{2+} cations, being shorter in length compared to BDA^{2+} , would ideally result in a slightly narrower $n = 4$ phase gap. However, the lattice distortion caused by EDA^{2+} is slightly greater than that induced by BDA^{2+} . These two factors compensate for each other, resulting in a nearly identical PL peak. From Figure 2b, it is clear that the PL peak of EDA is significantly higher than BDA. This is because the shorter chain length of EDA^{2+} reduces the distance between inorganic layers in quasi-2D perovskite and weakens the quantum confinement effect and dielectric confinement in quasi-2D perovskite. This results in lower exciton binding energy, which is beneficial for improving the carrier separation rate in quasi-2D perovskite [49].

As shown in the Time-Resolved Photoluminescence (TRPL) spectra of perovskite films in Figure 2c, the decay of PDA perovskite films is the most rapid, and the attenuation curves of BDA and EDA do not have many differences. The fluorescence lifetimes of the BDA, PDA, and EDA films were 3.6 ns, 1.9 ns, and 3.5 ns, respectively. The fluorescence lifetime of PDA can also be attributed to the decrease in radiation recombination due to the lattice distortion caused by organic spacer cations. The lattice distortion caused by BDA^{2+} is slightly less than that caused by EDA^{2+} . The difference in fluorescence lifetime between BDA and EDA also verifies the above conclusion.

In order to analyze the effect of organic spacers of different lengths on quasi-2D perovskite further, we collected the transient absorption spectra of three perovskite film samples. As shown in Figure 3, the transient absorption spectrum mainly consists of two parts; the positive signal of the transient absorption spectrum is a broad peak covering a range of tens of nanometers, and the negative signal in the transient absorption spectrum

is the ground-state bleaching signal (GSB) of the $n = 4$ phase. Although the broad peaks are in the form of positive signals, they also contain GSB signals of two-dimensional and three-dimensional phases. The intensity of the excited-state absorption (ESA) signal is stronger than the intensity of the GSB signal, so the ESA signal covers the negative signal of the ground-state bleaching signal, and the transient absorption spectrum shows as a positive signal. In addition, the Stark effect is also one of the reasons why the GSB signal of the two-dimensional and three-dimensional phases is covered. The positive signal mainly appears around the GSB signal of the $n = 4$ phase, which is caused by the absorption change of material under the influence of the electric field [50–52]. It is obvious that the transient absorption spectra under positive excitation are much weaker than those under negative excitation. In combination with PL spectra and the above analysis, the reason for the above phenomenon is that the density of states at the bottom of the perovskite film is higher than that at the top of the film. In the process of preparing perovskite films by spin coating the perovskite precursor solution, the perovskite films began to crystallize at the liquid–gas interface. However, due to the influence of gravity, the quasi-2D phase, which should be uniformly distributed, is inevitably deposited, and the density of states at the bottom of the perovskite film increases.

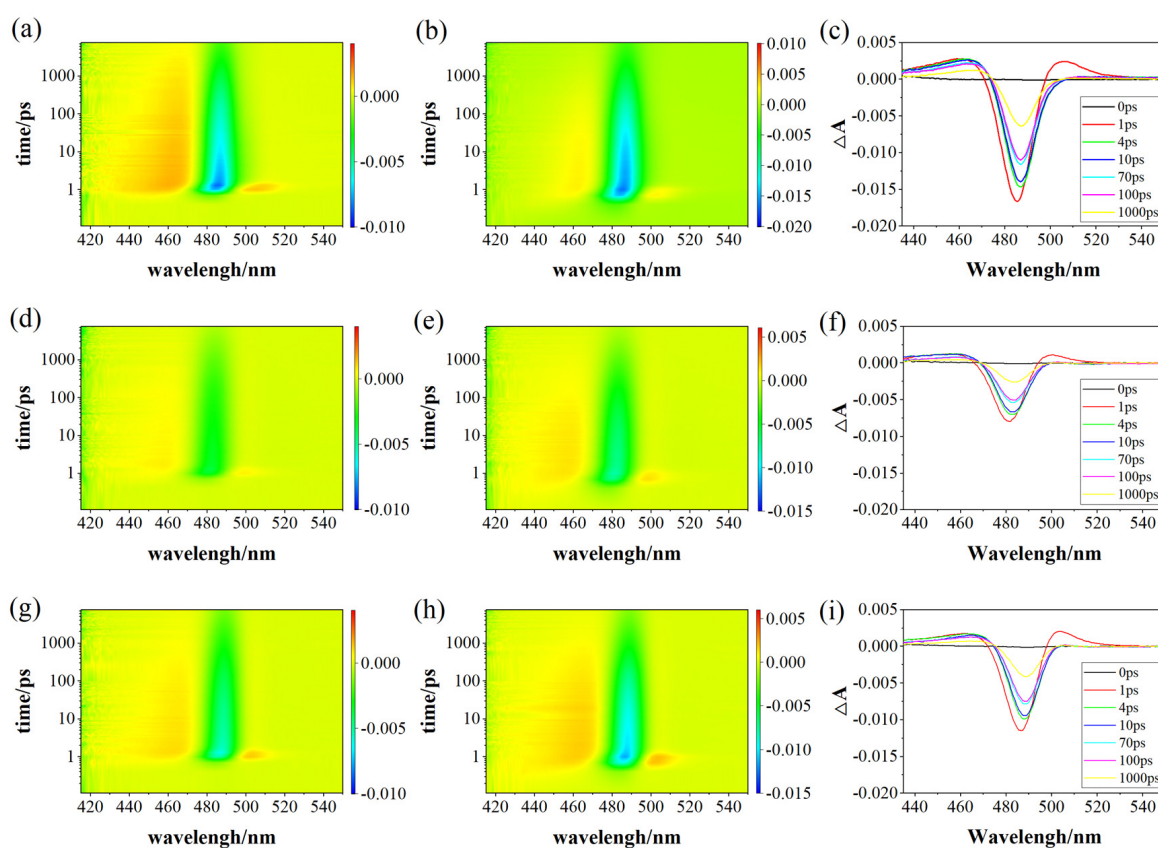


Figure 3. (a,b) are transient absorption spectra of EDA pumped front and back. (d,e) are transient absorption spectra of PDA pumped front and back. (g,h) are transient absorption spectra of BDA pumped front and back. (c,f,i) are transient absorption spectra of EDA, PDA, and BDA pumped back with different time delays.

The transient absorption spectra under positive excitation for perovskite films exhibit similarities to those under negative excitation. We extracted the transient absorption spectra for both top-excited and bottom-excited films, and the results are presented in Figure 4a and 4b, respectively. Moreover, the relationship between the transient absorption spectra of different organic spacer cationic perovskite materials excited from the top and bottom of the film is also similar. The time constants of monomolecular recombination

(defect recombination), bimolecular recombination (radiation recombination), and auger recombination can be obtained by three-exponential fitting of the transient absorption attenuation [53,54]. The fitting formula is shown below.

$$y = C_0 + C_1e^{-\frac{x}{\tau_1}} + C_2e^{-\frac{x}{\tau_2}} + C_3e^{-\frac{x}{\tau_3}}$$

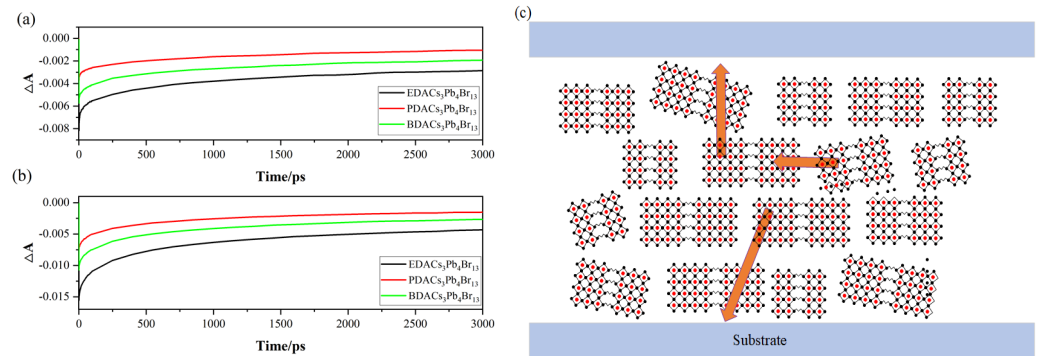


Figure 4. (a,b) Attenuation of transient absorption signals of EDA, PDA, and BDA excited from the top and bottom of the film. (c) Schematic diagram of energy transfer in perovskite thin films.

According to the time constants, the average carrier lifetime of different samples can be obtained. The average carrier lifetimes of EDA, PDA, and BDA are 2.11 ns, 2.37 ns, and 2.35 ns, respectively. The average carrier lifetime is calculated as follows:

$$\tau = \frac{C_1\tau_1^2 + C_2\tau_2^2 + C_3\tau_3^2}{C_1\tau_1 + C_2\tau_2 + C_3\tau_3}$$

The transient absorption signal intensity of the EDA samples is the highest of the three samples, and the second is the BDA samples. As shown in Figure 2a, the $n = 4$ exciton absorption peaks of the three samples are very close, which means that the $n = 4$ phase contents of the three perovskite films are close. As shown in Figure 4a, the enhancement of the transient absorption spectrum signal is accomplished in an extreme time. In such a short period of time, the trap has a limited effect on it. It can be inferred that the difference in the transient absorption spectrum signals of the three perovskite films mainly comes from ways other than the carrier generated by the $n = 4$ phase itself. We attribute the signal difference mainly to the energy transfer of perovskite from the small- n -value phase to the large- n -value phase. The transient absorption signal of three perovskite films was enhanced to the maximum within 1 ps, and the rising time of the signal was the same. It is obvious that the rising speed of the three samples is EDA > BDA > PDA. If the sample is excited from the top of the film, the rise time of the transient absorption spectrum signal is 0.5 ps longer than that from the bottom of the film. The EDA sample shows a faster and smoother energy-transfer process, which is mainly related to two factors. First, the EDA perovskite sample has a more favorable energy landscape for energy transfer, which can be seen from UV to Vis. The second is that EDA²⁺ has the shortest chain length among the three, which means that the distance between the inorganic layers of the low-dimensional phase in the EDA perovskite film sample is shorter than that between PDA and BDA. The shorter barrier reduces the quantum confinement effect and the dielectric confinement effect in the low-dimensional phase and weakens the effect of carriers being trapped in the inorganic layer. The PDA is supposed to have a stronger energy transfer than the BDA, but, in fact, it is the opposite. We think it is related to perovskite lattice distortion caused by PDA²⁺. The lattice distortion in perovskite leads to the increase in the low-dimensional interphase barrier of perovskite. The increased barrier due to lattice distortion is even longer than the barrier when the organic cations are PDA²⁺ and BDA²⁺. Therefore, the energy-transfer efficiency in PDA perovskite films is significantly reduced. Although EDA²⁺ and BDA²⁺

organic spacer cations also cause perovskite lattice distortion, the degree of lattice distortion of perovskites is not as severe as that of PDA.

We can conclude a carrier transfer model of quasi-2D perovskite materials. After being excited by light, perovskite materials rapidly transition from the ground state to the excited state and produce a large number of hot carriers. Then, these hot carriers will move in the same n value phase and from small- n phases (wide band gap) to large- n phase (narrow band gap). The latter process is mainly related to two factors: the energy landscape of perovskite materials and the quantum confinement effect in perovskite materials. In several picoseconds after photoexcitation, the carriers also transfer rapidly to the perovskite phase, resulting in a population inversion and ASE signal in a very short time.

We have recorded the PL spectra of perovskite thin films at different locations of the pump light spot. It can be seen from Figure 5 that the PL peak value at the center of the pump light spot is generally stronger than that at the edge of the pump spot. This is related to the concentration of the carrier at the measurement spot. By comparing the PL peak at the edge of the area and the PL peak at the center of the area in different perovskite samples, we can obtain the result as shown in Figure 5. The attenuation of carrier concentration from the center of the spot to the edge of the EDA sample is the smallest, while that of PDA is the strongest. This means that the carrier transfer process in EDA samples is superior to that in BDA and PDA, which is in agreement with the conclusions obtained above.

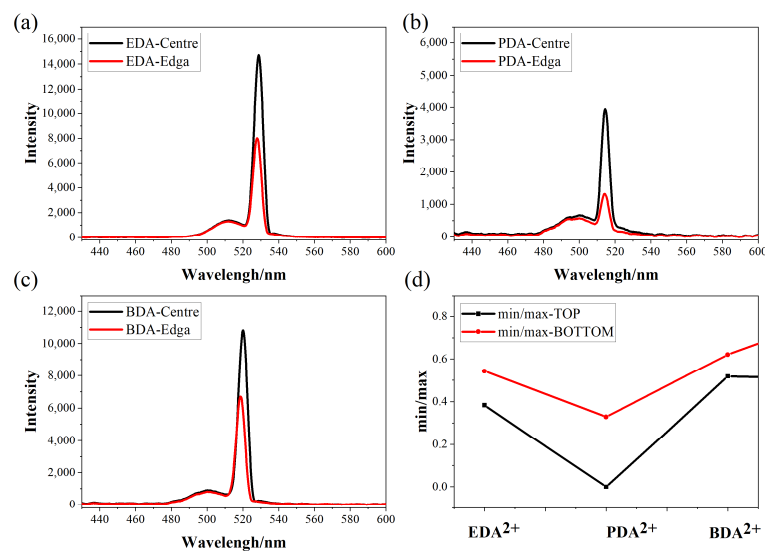


Figure 5. (a–c) The PL spectrums of EDA, PDA, and BDA are excited from the top and bottom of the films. (d) The ratio of the PL emission peak at the edge of the pump light spot to the central emission peak.

Although EDA perovskite has some advantages in fluorescence and energy transfer, it has a disadvantage that cannot be ignored compared to BDA and PDA. As seen in Figure 6, the transient absorption and fluorescence signals of EDA perovskite samples show a serious redshift (25.96 nm) after a while. This means that many of the original quasi-2D phases in EDA perovskite samples no longer have low-dimensional characteristics. The connection between the EDA²⁺ organic cation and the inorganic plate has been broken. Although the PDA sample and BDA sample also have a certain degree of redshift (PDA: 7.67 nm, BDA: 7.65 nm), compared with the EDA sample, the redshift of the PDA and BDA samples is not large. As shown in the picture, the degree of redshift of the PDA and BDA samples was the same. The result shows that the stability of the PDA and BDA samples is higher than that of the EDA sample.

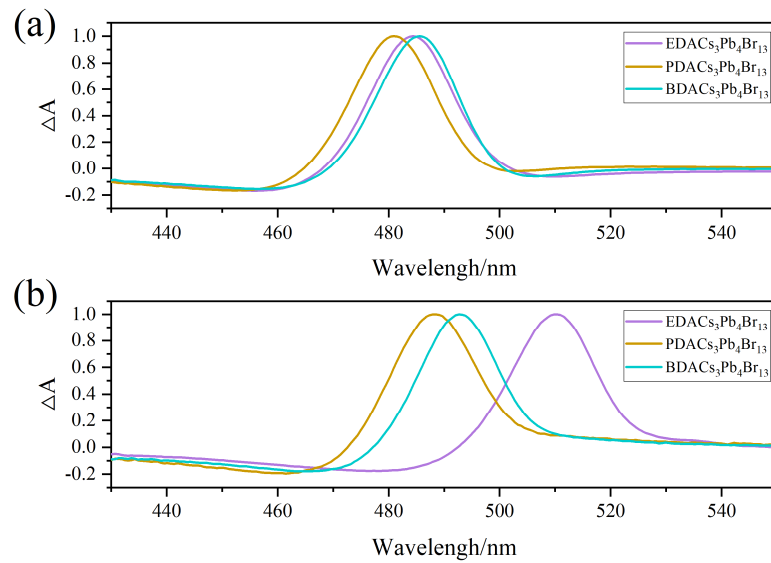


Figure 6. EDA, PDA, and BDA transient absorption signal after normalization: (a) initial stage of sample preparation, (b) 10 days after sample preparation.

3. Discussion

Based on the aforementioned experiments, the paper delves into the impact of organic spacer cations on perovskite. Notably, it was observed that shorter organic spacers result in reduced distances between inorganic layers. The organic cations follow the order of $\text{EDA}^{2+} < \text{PDA}^{2+} < \text{BDA}^{2+}$ in terms of length, with shorter lengths indicating smaller barriers and enhanced performance. However, barrier width is not the sole factor influencing perovskite performance. The two ends of the organic spacer extend into the connected inorganic layer, and the extent of this extension directly affects perovskite stability and lattice distortion.

As evidenced above, lattice distortion induced by PDA^{2+} is considerably greater than that caused by EDA^{2+} and BDA^{2+} [49]. Lattice distortion, in turn, alters the length of the Pb–Br bond, impacting the perovskite’s band gap. Simultaneously, lattice distortion plays a role in modifying the barrier width to some degree. This phenomenon results in a larger band gap, diminished luminescence properties, and weaker energy transfer for PDA, as depicted in Figures 2 and 4.

The organic spacer EDA^{2+} has the shortest length, allowing it to penetrate the inorganic layer to a limited extent. Consequently, EDA exhibits a narrower barrier and superior performance. However, the shorter penetration distance compromises the stability of the connection between organic spacer cations and the inorganic layer in EDA, making it less stable compared to PDA and BDA, a trend consistent with Figure 6.

4. Materials and Methods

Perovskite thin film: The precursor solution was prepared according to the ratios of $\text{CsBr}:\text{PbBr}_2:\text{EDABr}_2 = 3:4:1$, $\text{CsBr}:\text{PbBr}_2:\text{PDABr}_2 = 3:4:1$, and $\text{CsBr}:\text{PbBr}_2:\text{BDABr}_2 = 3:4:1$. Dimethyl Sulfoxide (DMSO) was used as a solvent in the sample. Quartz flakes were cleaned with ethanol. The quartz sheet was then illuminated with ultraviolet light (UVO) for 15 min. The precursor solution was then spun onto the quartz sheet. Finally, the samples were annealed and encapsulated. The film was prepared using the spin-coating method and annealed at 70 °C.

Film characterization: The UV–Vis spectra of the films were obtained using the New Century T6 UV–Vis spectrophotometer. TRPL spectra were obtained using the Lifespec II instrument system. The transient absorption spectra of the thin films were measured by a self-built transient absorption spectroscopy system. The central wavelength of the laser

was 800 nm, and the repetition frequency was 1 kHz. The pulse width of the laser used in the experiment was 40 fs. The system can achieve femtosecond time resolution.

5. Conclusions

In this study, quasi-2D perovskites featuring organic spacer cations of varying chain lengths were investigated. However, due to distortion effects, PDACs₃Pb₄Br₁₃ and BDACs₃Pb₄Br₁₃ samples were explicitly prepared for experiments. Notably, EDACs₃Pb₄Br₁₃, with the shortest organic isolation cation, exhibited weaker quantum-limiting effects and dielectric limiting compared to the other two samples. Remarkably, under identical excitation intensity, EDACs₃Pb₄Br₁₃ demonstrated a more vigorous luminous intensity. Additionally, in the short time following light excitation, EDACs₃Pb₄Br₁₃ exhibited faster carrier accumulation. If we consider the influence of organic spacer cation chain length on perovskite materials, the performance of the PDACs₃Pb₄Br₁₃ sample would be expected to surpass that of the BDACs₃Pb₄Br₁₃ sample. However, the distortion on the perovskite lattice caused by the PDA²⁺ organic spacer cation resulted in a decrease in the performance level of PDACs₃Pb₄Br₁₃ compared to its expected level. Furthermore, experimental results confirmed that the luminescence performance and energy transfer of PDACs₃Pb₄Br₁₃ were weaker than those of BDACs₃Pb₄Br₁₃. Despite the advantages exhibited by the EDACs₃Pb₄Br₁₃ perovskite sample over BDACs₃Pb₄Br₁₃, it was observed that the stability of the BDACs₃Pb₄Br₁₃ sample was significantly higher than that of the EDACs₃Pb₄Br₁₃. This suggests that, while EDACs₃Pb₄Br₁₃ may show favorable characteristics in certain aspects, the long-term stability of BDACs₃Pb₄Br₁₃ makes it a more promising candidate for practical applications.

Author Contributions: Conceptualization, Y.X. and L.S.; methodology, L.Z.; software, L.Z.; validation, L.Z. and Y.Z. (Yuan Zhang); resources, L.S. and X.G.; data curation, L.Z.; writing—original draft preparation, L.Z.; writing—review and editing, M.X. and Y.Z. (Yuan Zhang); visualization, M.X.; supervision, Y.Z. (Yong Zhang) and Y.W.; project administration, Y.X.; funding acquisition, Y.X. All authors have read and agreed to the published version of the manuscript.

Funding: This research was funded by The National Nature Science Foundation of China (62375074, 62075056) and The Nature Science Foundation of Hebei Province in China (F2021202055, F2022202035).

Data Availability Statement: The data presented in this study are available in this article.

Conflicts of Interest: Author Mingze Xia was employed by the company Cnooc Energy Technology and Services. The remaining authors declare that the research was conducted in the absence of any commercial or financial relationships that could be construed as potential conflicts of interest.

References

1. Stranks, S.D.; Snaith, H.J. Metal-halide perovskites for photovoltaic and light-emitting devices. *Nat. Nanotechnol.* **2015**, *10*, 391–402. [[CrossRef](#)] [[PubMed](#)]
2. Huang, P.; Kazim, S.; Wang, M.; Ahmad, S. Toward Phase Stability: Dion–Jacobson Layered Perovskite for Solar Cells. *ACS Energy Lett.* **2019**, *4*, 2960–2974. [[CrossRef](#)]
3. Zhao, W.; Dong, Q.; Zhang, J.; Wang, S.; Chen, M.; Zhao, C.; Hu, M.; Jin, S.; Padture, N.P.; Shi, Y. Asymmetric alkyl diamine based Dion–Jacobson low-dimensional perovskite solar cells with efficiency exceeding 15%. *J. Mater. Chem. A* **2020**, *8*, 9919–9926. [[CrossRef](#)]
4. He, T.; Li, S.; Jiang, Y.; Qin, C.; Cui, M.; Qiao, L.; Xu, H.; Yang, J.; Long, R.; Wang, H.; et al. Reduced-dimensional perovskite photovoltaics with homogeneous energy landscape. *Nature* **2020**, *11*, 1672. [[CrossRef](#)] [[PubMed](#)]
5. Fu, S.; Li, X.; Wan, L.; Zhang, W.; Song, W.; Fang, J. Effective Surface Treatment for High-Performance Inverted CsPbI₂Br Perovskite Solar Cells with Efficiency of 15.92. *Nanomicro Lett.* **2020**, *12*, 170. [[CrossRef](#)] [[PubMed](#)]
6. Fu, P.; Liu, Y.; Yu, S.; Yin, H.; Yang, B.; Ahmad, S.; Guo, X.; Li, C. Dion–Jacobson and Ruddlesden–Popper double-phase 2D perovskites for solar cells. *Nano Energy* **2021**, *88*, 106249. [[CrossRef](#)]
7. Yang, J.; Yang, T.; Liu, D.; Zhang, Y.; Luo, T.; Lu, J.; Fang, J.; Wen, J.; Deng, Z.; Liu, S.; et al. Stable 2D Alternating Cation Perovskite Solar Cells with Power Conversion Efficiency >19% via Solvent Engineering. *Sol. RRL* **2021**, *5*, 2100286. [[CrossRef](#)]
8. Zhang, Y.; Wen, J.; Xu, Z.; Liu, D.; Yang, T.; Niu, T.; Luo, T.; Lu, J.; Fang, J.; Chang, X.; et al. Effective Phase-Alignment for 2D Halide Perovskites Incorporating Symmetric Diammonium Ion for Photovoltaics. *Adv. Sci.* **2021**, *8*, 2001433. [[CrossRef](#)]

9. Ren, G.; Yan, C.; Xiao, L.; Wu, X.; Peng, S.; Lin, W.; Tan, W.; Liu, Y.; Min, Y. Additive-Induced Film Morphology Evolution for Inverted Dion–Jacobson Quasi-Two-Dimensional Perovskite Solar Cells with Enhanced Performance. *ACS Appl. Energy Mater.* **2022**, *5*, 9837–9845. [[CrossRef](#)]
10. Yang, Z.; Liu, Z.; Ahmadi, V.; Chen, W.; Qi, Y. Recent Progress on Metal Halide Perovskite Solar Minimodules. *Sol. RRL* **2022**, *6*, 2100458. [[CrossRef](#)]
11. Li, M.; Gao, Q.; Liu, P.; Liao, Q.; Zhang, H.; Yao, J.; Hu, W.; Wu, Y.; Fu, H. Amplified Spontaneous Emission Based on 2D Ruddlesden–Popper Perovskites. *Adv. Funct. Mater.* **2018**, *28*, 1707006. [[CrossRef](#)]
12. Yu, M.; Yi, C.; Wang, N.; Zhang, L.; Zou, R.; Tong, Y.; Chen, H.; Cao, Y.; He, Y.; Wang, Y.; et al. Control of Barrier Width in Perovskite Multiple Quantum Wells for High Performance Green Light-Emitting Diodes. *Adv. Opt. Mater.* **2018**, *7*, 1801575. [[CrossRef](#)]
13. Chen, P.; Meng, Y.; Ahmadi, M.; Peng, Q.; Gao, C.; Xu, L.; Shao, M.; Xiong, Z.; Hu, B. Charge-transfer versus energy-transfer in quasi-2D perovskite light-emitting diodes. *Nano Energy* **2018**, *50*, 615–622. [[CrossRef](#)]
14. Das, S.; Gholipour, S.; Saliba, M. Perovskites for Laser and Detector Applications. *Energy Environ. Mater.* **2019**, *2*, 146–153. [[CrossRef](#)]
15. Li, Z.; Chen, Z.; Yang, Y.; Xue, Q.; Yip, H.L.; Cao, Y. Modulation of recombination zone position for quasi-two-dimensional blue perovskite light-emitting diodes with efficiency exceeding 5. *Nat. Commun.* **2019**, *10*, 1027. [[CrossRef](#)]
16. Zhu, L.; Liu, D.; Wang, J.; Wang, N. Large Organic Cations in Quasi-2D Perovskites for High-Performance Light-Emitting Diodes. *J. Phys. Chem. Lett.* **2020**, *11*, 8502–8510. [[CrossRef](#)]
17. De Giorgi, M.L.; Creti, A.; La-Placa, M.G.; Boix, P.P.; Bolink, H.J.; Lomascolo, M.; Anni, M. Amplified spontaneous emission in thin films of quasi-2D BA3MA3Pb5Br16 lead halide perovskites. *Nanoscale* **2021**, *13*, 8893–8900. [[CrossRef](#)]
18. Kar, S.; Jamaludin, N.F.; Yantara, N.; Mhaisalkar, S.G.; Leong, W.L. Recent advancements and perspectives on light management and high performance in perovskite light-emitting diodes. *Nanophotonics* **2021**, *10*, 2103–2143. [[CrossRef](#)]
19. Lian, Y.; Yang, Y.; He, L.; Yang, X.; Gao, J.; Qin, C.; Niu, L.; Yang, X. Enhancing the Luminance Efficiency of Formamidinium-Based Dion–Jacobson Perovskite Light-Emitting Diodes via Compositional Engineering. *ACS Appl. Mater. Interfaces* **2021**, *14*, 1659–1669. [[CrossRef](#)]
20. Qin, X.; Liu, F.; Leung, T.L.; Sun, W.; Chan, C.C.S.; Wong, K.S.; Kanižaj, L.; Popović, J.; Djurišić, A.B. Compositional optimization of mixed cation Dion–Jacobson perovskites for efficient green light emission. *J. Mater. Chem. C* **2022**, *10*, 108–114. [[CrossRef](#)]
21. Lian, Y.; Yang, Y.; Gao, J.; Qin, C. Efficient Dion–Jacobson perovskite light-emitting diodes via mixed cation engineering. *Opt. Lett.* **2022**, *47*, 657–660. [[CrossRef](#)] [[PubMed](#)]
22. Zhong, Y.; Liu, G.; Su, Y.; Sheng, W.; Gong, L.; Zhang, J.; Tan, L.; Chen, Y. Diammonium molecular configuration-induced regulation of crystal orientation and carrier dynamics for highly efficient and stable 2D/3D perovskite solar cells. *Angew. Chem. Int. Ed.* **2022**, *61*, e202114588. [[CrossRef](#)] [[PubMed](#)]
23. Yu, H.; Xie, Y.; Zhang, J.; Duan, J.; Chen, X.; Liang, Y.; Wang, K.; Xu, L. Thermal and humidity stability of mixed spacer cations 2D perovskite solar cells. *Adv. Sci.* **2021**, *8*, 2004510. [[CrossRef](#)] [[PubMed](#)]
24. Xu, J.; Chen, J.; Chen, S.; Gao, H.; Li, Y.; Jiang, Z.; Zhang, Y.; Wang, X.; Zhu, X.; Xu, B. Organic spacer engineering of ruddlesden–popper perovskite materials toward efficient and stable solar cells. *Chem. Eng. J.* **2023**, *453*, 139790. [[CrossRef](#)]
25. Yang, T.; Ma, C.; Cai, W.; Wang, S.; Wu, Y.; Feng, J.; Wu, N.; Li, H.; Huang, W.; Ding, Z. Amidino-based Dion–Jacobson 2D perovskite for efficient and stable 2D/3D heterostructure perovskite solar cells. *Joule* **2023**, *7*, 574–586. [[CrossRef](#)]
26. Ngai, K.H.; Wei, Q.; Chen, Z.; Guo, X.; Qin, M.; Xie, F.; Chan, C.C.S.; Xing, G.; Lu, X.; Chen, J. Enhanced electrochemical stability by alkyldiammonium in Dion–Jacobson perovskite toward ultrastable light-emitting diodes. *Adv. Opt. Mater.* **2021**, *9*, 2100243. [[CrossRef](#)]
27. Lei, Y.; Li, Z.; Wang, H.; Wang, Q.; Peng, G.; Xu, Y.; Zhang, H.; Wang, G.; Ding, L.; Jin, Z. Manipulate energy transport via fluorinated spacers towards record-efficiency 2D Dion–Jacobson CsPbI3 solar cells. *Sci. Bull.* **2022**, *67*, 1352–1361. [[CrossRef](#)] [[PubMed](#)]
28. Ke, W.; Mao, L.; Stoumpos, C.C.; Hoffman, J.; Spanopoulos, I.; Mohite, A.D.; Kanatzidis, M.G. Compositional and solvent engineering in Dion–Jacobson 2D perovskites boosts solar cell efficiency and stability. *Adv. Energy Mater.* **2019**, *9*, 1803384. [[CrossRef](#)]
29. Wu, H.; Lian, X.; Tian, S.; Zhang, Y.; Qin, M.; Zhang, Y.; Wang, F.; Lu, X.; Wu, G.; Chen, H. Additive-Assisted Hot-Casting Free Fabrication of Dion–Jacobson 2D Perovskite Solar Cell with Efficiency Beyond 16%. *Sol. RRL* **2020**, *4*, 2000087. [[CrossRef](#)]
30. Mitzi, D.B. Templating and structural engineering in organic–inorganic perovskites. *J. Chem. Soc. Dalton Trans.* **2001**, *1*, 1–12. [[CrossRef](#)]
31. Hu, T.; Smith, M.D.; Dohner, E.R.; Sher, M.-J.; Wu, X.; Trinh, M.T.; Fisher, A.; Corbett, J.; Zhu, X.Y.; Karunadasa, H.I. Mechanism for broadband white-light emission from two-dimensional (110) hybrid perovskites. *J. Phys. Chem. Lett.* **2016**, *7*, 2258–2263. [[CrossRef](#)] [[PubMed](#)]
32. Tan, M.; Wang, S.; Rao, F.; Yang, S.; Wang, F. Pressures tuning the band gap of organic–inorganic trihalide perovskites (MAPbBr3): A first-principles study. *J. Electron. Mater.* **2018**, *47*, 7204–7211. [[CrossRef](#)]
33. Mao, L.; Guo, P.; Kepenekian, M.; Hadar, I.; Katan, C.; Even, J.; Schaller, R.D.; Stoumpos, C.C.; Kanatzidis, M.G. Structural diversity in white-light-emitting hybrid lead bromide perovskites. *J. Am. Chem. Soc.* **2018**, *140*, 13078–13088. [[CrossRef](#)] [[PubMed](#)]

34. Saidaminov, M.I.; Mohammed, O.F.; Bakr, O.M. Low-dimensional-networked metal halide perovskites: The next big thing. *ACS Energy Lett.* **2017**, *2*, 889–896. [[CrossRef](#)]
35. Ahmad, S.; Hanmandlu, C.; Kanaujia, P.K.; Prakash, G.V. Direct deposition strategy for highly ordered inorganic organic perovskite thin films and their optoelectronic applications. *Opt. Mater. Express* **2014**, *4*, 1313–1323. [[CrossRef](#)]
36. Hong, X.; Ishihara, T.; Nurmikko, A.V. Dielectric confinement effect on excitons in Pbl 4-based layered semiconductors. *Phys. Rev. B* **1992**, *45*, 6961. [[CrossRef](#)] [[PubMed](#)]
37. Muljarov, E.A.; Tikhodeev, S.G.; Gippius, N.A.; Ishihara, T. Excitons in self-organized semiconductor/insulator superlattices: Pbl-based perovskite compounds. *Phys. Rev. B* **1995**, *51*, 14370. [[CrossRef](#)] [[PubMed](#)]
38. Chen, Y.; Sun, Y.; Peng, J.; Zhang, W.; Su, X.; Zheng, K.; Pullerits, T.; Liang, Z. Tailoring organic cation of 2D air-stable organometal halide perovskites for highly efficient planar solar cells. *Adv. Energy Mater.* **2017**, *7*, 1700162. [[CrossRef](#)]
39. Guo, X.; Gao, Y.; Wei, Q.; Ho Ngai, K.; Qin, M.; Lu, X.; Xing, G.; Shi, T.; Xie, W.; Xu, J. Suppressed Phase Segregation in High-Humidity-Processed Dion–Jacobson Perovskite Solar Cells Toward High Efficiency and Stability. *Sol. RRL* **2021**, *5*, 2100555. [[CrossRef](#)]
40. Proppe, A.H.; Quintero-Bermudez, R.; Tan, H.; Voznyy, O.; Kelley, S.O.; Sargent, E.H. Synthetic control over quantum well width distribution and carrier migration in low-dimensional perovskite photovoltaics. *J. Am. Chem. Soc.* **2018**, *140*, 2890–2896. [[CrossRef](#)]
41. Li, X.; Hoffman, J.; Ke, W.; Chen, M.; Tsai, H.; Nie, W.; Mohite, A.D.; Kepenekian, M.; Katan, C.; Even, J. Two-dimensional halide perovskites incorporating straight chain symmetric diammonium ions, $(\text{NH}_3\text{C}_m\text{H}_{2m}\text{NH}_3)(\text{CH}_3\text{NH}_3)_{n-1}\text{Pb}_n\text{I}_{3n+1}$ ($m = 4-9$; $n = 1-4$). *J. Am. Chem. Soc.* **2018**, *140*, 12226–12238. [[CrossRef](#)] [[PubMed](#)]
42. Ma, C.; Shen, D.; Ng, T.W.; Lo, M.F.; Lee, C.S. 2D perovskites with short interlayer distance for high-performance solar cell application. *Adv. Mater.* **2018**, *30*, 1800710. [[CrossRef](#)] [[PubMed](#)]
43. Ahmad, S.; Fu, P.; Yu, S.; Yang, Q.; Liu, X.; Wang, X.; Wang, X.; Guo, X.; Li, C. Dion–Jacobson phase 2D layered perovskites for solar cells with ultrahigh stability. *Joule* **2019**, *3*, 794–806. [[CrossRef](#)]
44. Zheng, Y.; Niu, T.; Qiu, J.; Chao, L.; Li, B.; Yang, Y.; Li, Q.; Lin, C.; Gao, X.; Zhang, C. Oriented and uniform distribution of Dion–Jacobson phase perovskites controlled by quantum well barrier thickness. *Sol. RRL* **2019**, *3*, 1900090. [[CrossRef](#)]
45. Sourisseau, S.; Louvain, N.; Bi, W.; Mercier, N.; Rondeau, D.; Boucher, F.; Buzaré, J.-Y.; Legein, C. Reduced band gap hybrid perovskites resulting from combined hydrogen and halogen bonding at the organic–inorganic interface. *Chem. Mater.* **2007**, *19*, 600–607. [[CrossRef](#)]
46. Gan, L.; Li, J.; Fang, Z.; He, H.; Ye, Z. Effects of organic cation length on exciton recombination in two-dimensional layered lead iodide hybrid perovskite crystals. *J. Phys. Chem. Lett.* **2017**, *8*, 5177–5183. [[CrossRef](#)]
47. Blancon, J.C.; Tsai, H.; Nie, W.; Stoumpos, C.C.; Pedesseau, L.; Katan, C.; Kepenekian, M.; Soe, C.M.M.; Appavoo, K.; Sfeir, M.Y. Extremely efficient internal exciton dissociation through edge states in layered 2D perovskites. *Science* **2017**, *355*, 1288–1292. [[CrossRef](#)]
48. Han, Y.; Li, Y.; Wang, Y.; Cao, G.; Yue, S.; Zhang, L.; Cui, B.B.; Chen, Q. From distortion to disconnection: Linear alkyl diammonium cations tune structure and photoluminescence of lead bromide perovskites. *Adv. Opt. Mater.* **2020**, *8*, 1902051. [[CrossRef](#)]
49. Ajayakumar, A.; Muthu, C.; Dev, A.V.; Pious, J.K.; Vijayakumar, C. Two-Dimensional Halide Perovskites: Approaches to Improve Optoelectronic Properties. *Chem.—Asian J.* **2022**, *17*, e202101075. [[CrossRef](#)]
50. Queloz, V.I.E.; Bouduban, M.E.F.; García-Benito, I.; Fedorovskiy, A.; Orlandi, S.; Cavazzini, M.; Pozzi, G.; Trivedi, H.; Lupascu, D.C.; Beljonne, D. Spatial charge separation as the origin of anomalous stark effect in fluorine 2d hybrid perovskites. *Adv. Funct. Mater.* **2020**, *30*, 2000228. [[CrossRef](#)]
51. Walters, G.; Wei, M.; Voznyy, O.; Quintero-Bermudez, R.; Kiani, A.; Smilgies, D.M.; Munir, R.; Amassian, A.; Hoogland, S.; Sargent, E. The quantum-confined Stark effect in layered hybrid perovskites mediated by orientational polarizability of confined dipoles. *Nat. Commun.* **2018**, *9*, 4214. [[CrossRef](#)] [[PubMed](#)]
52. Sharma, D.K.; Hirata, S.; Biju, V.; Vacha, M. Stark effect and environment-induced modulation of emission in single halide perovskite nanocrystals. *ACS Nano* **2019**, *13*, 624–632. [[CrossRef](#)] [[PubMed](#)]
53. Manser, J.S.; Kamat, P.V. Band filling with free charge carriers in organometal halide perovskites. *Nat. Photonics* **2014**, *8*, 737–743. [[CrossRef](#)]
54. Konidakis, I.; Maksudov, T.; Serpetzoglou, E.; Kakavelakis, G.; Kymakis, E.; Stratakis, E. Improved Charge Carrier Dynamics of $\text{CH}_3\text{NH}_3\text{PbI}_3$ Perovskite Films Synthesized by Means of Laser-Assisted Crystallization. *ACS Appl. Energy Mater.* **2018**, *1*, 5101–5111. [[CrossRef](#)]

Disclaimer/Publisher’s Note: The statements, opinions and data contained in all publications are solely those of the individual author(s) and contributor(s) and not of MDPI and/or the editor(s). MDPI and/or the editor(s) disclaim responsibility for any injury to people or property resulting from any ideas, methods, instructions or products referred to in the content.